Geosci. Model Dev., 10, 2303–2320, 2017
https://doi.org/10.5194/gmd-10-2303-2017

Geoscientific Model Development
Open Access
EGU

Constraining a hybrid volatility basis-set model for aging of wood-burning emissions using smog chamber experiments: a box-model study based on the VBS scheme of the CAMx model (v5.40)

Giancarlo Ciarelli[1,a], Imad El Haddad[1], Emily Bruns[1], Sebnem Aksoyoglu[1], Ottmar Möhler[2], Urs Baltensperger[1], and André S. H. Prévôt[1]

[1]Laboratory of Atmospheric Chemistry, Paul Scherrer Institute, 5232 Villigen PSI, Switzerland
[2]Institute of Meteorology and Climate Research, Karlsruhe Institute of Technology, Karlsruhe, Germany
[a]now at: Laboratoire Inter-Universitaire des Systèmes Atmosphériques (LISA), UMR CNRS 7583, Université Paris Est Créteil et Université Paris Diderot, Institut Pierre Simon Laplace, Créteil, France

Correspondence to: Imad El Haddad (imad.el-haddad@psi.ch) and Sebnem Aksoyoglu (sebnem.aksoyoglu@psi.ch)

Received: 24 June 2016 – Discussion started: 11 August 2016
Revised: 10 March 2017 – Accepted: 26 March 2017 – Published: 23 June 2017

Abstract. In this study, novel wood combustion aging experiments performed at different temperatures (263 and 288 K) in a $\sim 7\,m^3$ smog chamber were modelled using a hybrid volatility basis set (VBS) box model, representing the emission partitioning and their oxidation against OH. We combine aerosol–chemistry box-model simulations with unprecedented measurements of non-traditional volatile organic compounds (NTVOCs) from a high-resolution proton transfer reaction mass spectrometer (PTR-MS) and with organic aerosol measurements from an aerosol mass spectrometer (AMS). Due to this, we are able to observationally constrain the amounts of different NTVOC aerosol precursors (in the model) relative to low volatility and semi-volatile primary organic material (OM_{sv}), which is partitioned based on current published volatility distribution data. By comparing the NTVOC / OM_{sv} ratios at different temperatures, we determine the enthalpies of vaporization of primary biomass-burning organic aerosols. Further, the developed model allows for evaluating the evolution of oxidation products of the semi-volatile and volatile precursors with aging. More than 30 000 box-model simulations were performed to retrieve the combination of parameters that best fit the observed organic aerosol mass and O : C ratios. The parameters investigated include the NTVOC reaction rates and yields as well as enthalpies of vaporization and the O : C of secondary organic aerosol surrogates. Our results suggest an average ratio of NTVOCs to the sum of non-volatile and semi-volatile organic compounds of ~ 4.75. The mass yields of these compounds determined for a wide range of atmospherically relevant temperatures and organic aerosol (OA) concentrations were predicted to vary between 8 and 30 % after 5 h of continuous aging. Based on the reaction scheme used, reaction rates of the NTVOC mixture range from 3.0×10^{-11} to 4.0×10^{-11} cm^3 $molec^{-1}$ s^{-1}. The average enthalpy of vaporization of secondary organic aerosol (SOA) surrogates was determined to be between 55 000 and 35 000 J mol^{-1}, which implies a yield increase of 0.03–0.06 % K^{-1} with decreasing temperature. The improved VBS scheme is suitable for implementation into chemical transport models to predict the burden and oxidation state of primary and secondary biomass-burning aerosols.

1 Introduction

The fact that some semi-volatile compounds can exist in either gaseous or particulate form results in considerable uncertainties in the emission inventories for primary organic aerosol (POA). Emissions of $PM_{2.5}$ are generally based on emission factors (EF) of POA, which may be over- or under-

predicted depending on the measurement method used (Lipsky and Robinson, 2006; Nussbaumer et al., 2008a, b).

In Europe, residential wood-burning emissions constitute one of the main anthropogenic sources of POA and potentially secondary organic aerosol (SOA), especially during winter periods with a contribution from 15 to 50 % of the total organic mass (Crippa et al., 2013; Waked et al., 2014). Thus, great effort was devoted in the past to better constrain the uncertainties related to wood-burning emissions and their evolution in the atmosphere (Denier van der Gon et al., 2015; May et al., 2013). Recent year-long source-apportionment studies based on ACSM (aerosol chemical speciation monitor) measurements in central Europe suggest that winter SOA fingerprints resembles those measured during chamber studies of biomass-burning emission aging (Canonaco et al., 2015).

One of the main complications when dealing with organic aerosol (OA) is imposed by the semi-volatile and highly reactive nature of organic material (Robinson et al., 2007). Depending on ambient conditions freshly emitted primary organic particles can undergo evaporation. Once emitted to the atmosphere, organic compounds are highly reactive towards various oxidants such as the hydroxyl radical (OH), ozone (O_3) and the nitrate radical (NO_3). These oxidants can strongly alter the chemical structure of the reacted precursors by generating secondary products with lower or higher volatilities. Linking partitioning and oxidation processes of thousands of emitted organic compounds is one of the main challenges in atmospheric chemistry. The volatility basis set (VBS) scheme can delineate the transformation of the surrogates upon their functionalization or fragmentation, by changing the compounds' volatility and O : C ratios, consistently with the dominant representative species in that part of the parameter space. Regional and global chemical transport models (CTMs) have been increasingly updated with a VBS scheme with varying complexities (Bergström et al., 2012; Ciarelli et al., 2016; Hodzic et al., 2016; Jathar et al., 2011; Murphy et al., 2011; Shrivastava et al., 2015; Tsimpidi et al., 2014; Zhang et al., 2013). A recent landmark paper within the international AeroCom initiative (Tsigaridis et al., 2014) gave a comprehensive audit of the status of organic aerosol schemes in global models, brought together several benchmark observational datasets and intercompared and evaluated the OA simulated by a large number of global aerosol models against them. Results indicate that simulated OA greatly varies between models in terms of POA emissions, SOA formation and complexity of OA parameterizations, but the amount of OA remains under-predicted. In the latest EURODELTA III (ED-III) European model intercomparison, seven different regional models were applied in the European domain during different periods (Bessagnet et al., 2016). All models under-predicted the total measured organic fraction during the February–March 2009 winter episode mainly due to the uncertainties in SOA representation (Bessagnet et al., 2014). Knote et al. (2011) used the COSMO-ART model to investigate its performance as online-coupled chemistry–climate model. In their study domestic wood-burning emissions were not included and POA was assumed to be non-volatile, which resulted in a severe under-prediction of OA over the studied domain (Knote et al., 2011). Fountoukis et al. (2014) were among the first to implement the VBS approach into a large-scale aerosol model, following the multiple distribution framework approach proposed by Tsimpidi et al. (2010). They found that the approach considerably improved the model result for OA when compared to a range of observations from the EUCAARI field campaign (Kulmala et al., 2009, 2011) and from EMEP monitoring network (Tørseth et al., 2012). Bergström et al. (2012) used the EMEP model for the period of 2002–2007 to compare different partitioning and aging schemes. Their results indicate the importance, although potential underestimation, of wood-burning emissions in Europe, in line with other studies (Kostenidou et al., 2013; Fountoukis et al., 2016; Tsimpidi et al., 2016). Recently, an important new initiative to provide improved information on residential wood combustion (RWC) emission inventory for Europe was carried out by Denier van der Gon et al. (2015) and used as input in two CTMs (PMCAMx and EMEP MSC-W) for the EUCAARI winter periods (February–March 2009). The new RWC emissions, which are higher by a factor of 2–3 compared to previous emission inventories, improved the model performance for total OA (Denier van der Gon et al., 2015). On the other hand, radiocarbon dating (Mohr et al., 2012; Zotter et al., 2014) and measurements of specific molecular markers, including methyl-nitrocatechols (Iinuma et al., 2010; El Haddad et al., 2013), during winter reveal the importance of residential wood burning for SOA formation. However, parameters needed for the simulation of the aging of biomass smoke remain not well constrained. These novel investigations highlight the critical need for a representation of semi-volatile organic species and their evolution in chemical transport models.

In this study we perform extensive box-model simulations of wood-burning combustion aging experiments performed in a $\sim 7\,m^3$ smog chamber at different temperatures. Most uncertain parameters namely enthalpies of vaporization of SOA, NTVOCs (non-traditional volatile organic compounds) reaction rates and their yields were investigated by means of a brute force approach, and a best-fitting solution, within acceptable physical limits and error ranges, was retrieved.

2 Experimental method

Beech (*Fagus sylvatica*) logs were combusted in a residential wood burner (model type: Avant, Attika from 2009), following the procedure described in Heringa et al. (2012) and Bruns et al. (2015). The resulting emissions were sampled from the chimney through a heated line (473 K), diluted by a factor of $\sim$ 8–10 using an ejector diluter (473 K, DI-1000,

Dekati Ltd.) and injected into the smog chamber ($\sim 7\,m^3$) through a heated line (423 K). Emissions were only sampled during the stable flaming phase of the burn, for 11–21 min and total dilution factors ranged from ~ 100 to 200. Four replicate experiments were conducted at 288 K and another four experiments at 263 K. The smog chamber had an average relative humidity (RH) of 50 % over all eight experiments. Another three experiments were conducted at 90 % relative humidity and 263 K. After the characterization of the primary emissions, a single dose of d9-butanol (butanol-D9, 98 %, Cambridge Isotope Laboratories) was injected into the chamber, to trace the OH concentration (Barmet et al., 2012). A continuous flow of nitrous acid (2.3–2.6 L min^{-1}, ≥ 99.999 %, Air Liquide) into the chamber served as an OH precursor. The chamber was then irradiated with UV light (40 lights, 90–100 W, Cleo Performance, Philips) for 4.5–6 h (Platt et al., 2013). The evolution of the gas-phase and particulate phase composition and concentration were monitored in real time throughout aging. Non-refractory primary and secondary particulate emissions were characterized using a high-resolution time-of-flight aerosol mass spectrometer (AMS). Equivalent black carbon (eBC) was quantified using a 7-wavelength aethalometer (AE33 Magee Scientific Company, flow rate 2 L min^{-1}) (Drinovec et al., 2015). Non-methane organic gases with a proton affinity greater than that of water were measured using a high-resolution proton transfer reaction mass spectrometer (PTR-ToF-MS 8000, Ionicon Analytik G.m.b.H.). The PTR-ToF-MS was operated with hydronium ($[H_2O + H]^+$) as reagent, a drift tube pressure of 2.2 mbar, a drift tube voltage of 543 V and a drift tube temperature of 90 °C leading to a ratio of the electric field (E) and the density of the buffer gas (N) in the drift tube (E/N) of 137 Townsend. The analysis of PTR-ToF-MS data and the identification of the precursors' chemical nature are described in Bruns et al. (2016). The elemental composition of the detected gases was analysed using the Tofware post-processing software (version 2.4.5), running in the Igor Pro 6.3 environment (version 6.3, Wavemetrics Inc.). More than 95 % of the detected peaks could be assigned to a molecular formula. Approximately 70 % of the compounds' chemical structures could be assigned to the observed ions guided by previously reported compounds emitted during the residential wood combustion. Here, the lumped sum of the precursors' molar concentrations will be used to constrain the total amount of NTVOCs (Table S1 in the Supplement) in the model. Their weighted average O : C ratio, volatility, reaction rate and carbon number will also be presented.

Particle wall loss rates in the chamber were determined using the decay of eBC assuming all particles were lost equally to the walls and condensable material partitions only to suspended particles. The average particle half-life in the chamber was 3.4 ± 0.7 h. NTVOCs were stable in the chamber prior to aging, indicating that the chamber walls are not an effective sink for NTVOCs (Bruns et al., 2016). This is because NTVOCs acting as SOA precursors are largely composed of volatile compounds (see below). By contrast, the NTVOC oxidation products are expected to be semi-volatile and partition to both the walls and the particles. Zhang et al. (2014) showed that the bias created by the wall loss is inversely proportional to the seed aerosol concentration and OH concentration, both of which were relatively high in the current experiments (Bruns et al., 2016). Therefore, under our experimental conditions, wall losses of NTVOC oxidation products are not expected to be large and thus this effect was not corrected for and yields presented should be considered as the lowest estimates.

3 Model description

The representation of SOA formation is based on the absorptive partitioning theory of Pankow (1994), assuming instantaneous reversible absorptive equilibrium. In this representation, the critical parameters driving the partitioning of a compound i between the gas and the condensed phases are its effective saturation concentration, C_i^*, and the total concentration of organic aerosol, C_{OA}:

$$\xi_i = \left(1 + \frac{C_i^*}{C_{OA}}\right)^{-1}; \quad C_{OA} = \sum_i \xi_i C_i. \tag{1}$$

Here, ξ_i is the partitioning coefficient of i (condensed-phase mass fraction). C_i^* is a semi-empirical property (inverse of the Pankow-type partitioning coefficient, K_P), reflecting not only the saturation vapour pressure of the pure constituents ($p^o_{L,i}$) but also the way they interact with the organic mixture (effectively including liquid phase activities). This formulation essentially implies that at high C_{OA} almost all semi-volatile organic aerosols are in the condensed phase with only species with the highest vapour pressures remaining in the gas phase.

The VBS approach proposed by Donahue et al. (2006) provides a framework for the representation of both the chemical aging and the associated volatility of particulate organic matter evolving in the atmosphere. The approach separates the organics into logarithmically spaced bins of effective saturation concentrations C_i^*, at 298 K. This has been later extended (Donahue et al., 2011, 2012) by introducing surrogate compounds with different carbon and oxygen numbers following the group contribution approach based on the SIMPOL method (Pankow and Asher, 2008) (Eq. 2).

$$\mathrm{Log}C_i^* = \left(n_C^0 - n_C^i\right) b_C - n_O^i b_O - 2\frac{n_C^i n_O^i}{n_C^i + n_O^i} b_{CO}, \tag{2}$$

where b_C and b_O represent the carbon–carbon and oxygen–oxygen interactions, respectively, b_{CO} describes the non-ideal solution behaviour and n_C^0, equal to 25, represents the reference point for pure hydrocarbons (1 µg m^{-3} of alkene). n_C^i and n_O^i are the carbon and oxygen numbers, respectively,

for the ith saturation concentration, at 298 K. In this configuration, the model becomes two-dimensional (2D-VBS), capable of tracking the volatility and oxidation state (O : C ratios) (Donahue et al., 2011, 2012) of oxidation products arising from functionalization and fragmentation of their precursors.

Here, we have used the VBS scheme proposed by Koo et al. (2014), referred to as a hybrid 1.5D-VBS and adapted for regional models. In this framework, the molecular space is not discretized according to the species saturation concentration and oxidation state, but rather every SOA surrogate is given an average molecular composition ($C_xH_yO_z$) – as a function of its volatility and the precursor it derives from. While a further simplification of the system compared to the 2D-VBS, this approach significantly decreases the degree of freedom of the model, while still providing means to evaluate the bulk aerosol oxidation state based on the knowledge of the surrogate molecular composition. This is especially suitable given the limited constraints available, namely the precursor composition, the precursor concentration, the POA concentration, the aged OA concentration and the O : C ratios.

In practice, five volatility bins ranging from 0.1 to 1000 $\mu g\,m^{-3}$ in saturation concentration were used to model the partitioning of the POA and SOA fractions. The weighted average carbon and oxygen numbers of the NTVOCs mixture retrieved from the PTR-ToF-MS measurements were used in combination with the group contribution approach (Eq. 2) to estimate the average saturation concentration for SOA precursors yielding $\sim 10^6\,\mu g\,m^{-3}$, which is at the high end of the intermediate volatility organic compound (IVOC) saturation concentration range (Donahue et al., 2012; Koo et al., 2014; Murphy and Pandis, 2009) (Table 1).

A total number of three sets were used to describe the organic material. The first set was used to distribute the primary emissions (set 1). Two other sets were used to model the formation and evolution of semi-volatile organic compounds (SVOCs). Oxidation products of SVOC material arising from primary emissions were allocated to set 2, whereas oxidation products from NTVOCs were allocated to set 3 (Fig. 1). The specific molecular structures for each of the sets and bins were retrieved using the group contribution approach and the Van Krevelen relation, as shown in Table 1 (Donahue et al., 2011; Heald et al., 2010).

Primary wood-burning emissions were placed to range from 14 to 11 carbons (set 1) in line with previous studies (Donahue et al., 2012; Koo et al., 2014) and appropriate numbers of oxygen atoms were retrieved using Eq. (2). The distribution of the primary organic material in the low-volatility ($C_i^* = 0.1\,\mu g\,m^{-3}$), and semi-volatile ranges (OM_{sv}) ($0.1 < C_i^* < 1000\,\mu g\,m^{-3}$) in set 1 (Table 1) is based on the work of May et al. (2013). This work revealed that the majority of the emitted primary organic mass is semi-volatile, with 50 to 80 % of the POA mass evaporating when diluted from plume to ambient concentrations or when heated up to 100 °C in a thermodenuder.

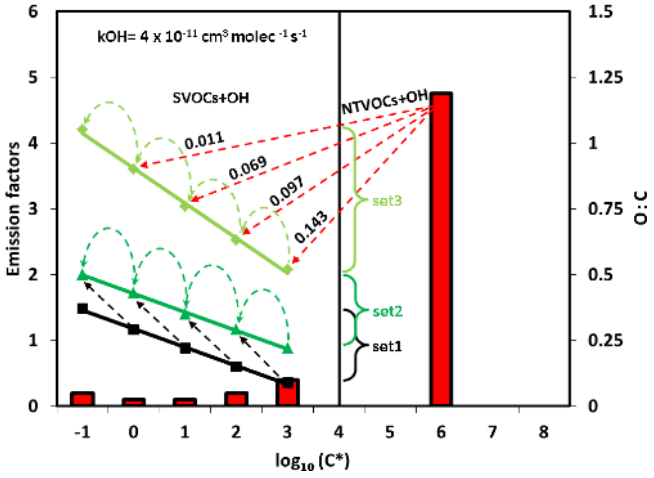

Figure 1. Proposed oxidation scheme: an average mixture of NTVOCs compounds are allowed to react with the hydroxyl radical following a naphthalene kernel mass distribution. Secondary products in the SOA set (set 3) are allowed to further react with a reaction rate of $k_{OH} = 4.0 \times 10^{-11}$ cm^3 $molec^{-1}$ s^{-1}. Oxidation products from semi-volatile vapours from the POA set (set 1) are allowed for further aging in set 2. The numbers on the red arrows indicate the NTVOCs yields for each bin for the best-fitting solution (ppm ppm^{-1}).

The oxidation of semi-volatile material would tend on average to increase the compounds' oxygen number and decrease their volatility and carbon number, due to functionalization and fragmentation. We assume that the oxidation of the primary semi-volatile compounds with C_{11}–C_{14} decreases their volatility by 1 order of magnitude and yields C_9–C_{10} surrogates, placed in set 2, based on the work of Donahue et al. (2011, 2012). Based on these assumptions and using the group contribution approach, the oxygen numbers for set 2 is predicted to vary between 2.26 and 4.56 (Table 1). Thus, the model implicitly accounts for the addition of 1.1 to 1.5 oxygen atoms and the loss of 2.75 to 4.25 carbon atoms, with one oxidation step.

Set 3 was constrained based on the proton transfer reaction mass spectrometer (PTR-MS) data. The measurements suggested an average NTVOC carbon and oxygen number of about 7 and 1, respectively. Based on reported molecular speciation data (e.g. Kleindienst et al., 2007), we expect the products of C_7 compounds to have a C_5–C_6 carbon backbone. These products were placed in set 3 following a kernel function based on the distribution of naphthalene oxidation products. At least two oxygen atoms were added to the NTVOC mixture upon their oxidation (Table 1). The overall O : C ratio in the whole space roughly spans the range of 0.1–1.0.

Multi-generation chemistry (aging) is also accounted for by the model. Unlike the 2D-VBS, the 1.5D-VBS does not

Table 1. Properties of the VBS space. Oxygen numbers for each volatility bin were calculated using the group contribution of Donahue et al. (2011). Hydrogen numbers were calculated from the van Krevelen relation (Heald et al., 2010).

	Log (C^*)	Oxygen number	Carbon number	Hydrogen number	O : C ratio	Molecular weight	Emission factors	ΔH J mol^{-1}
POA set 1	−1	4.11	11.00	17.89	0.37	216	0.2	–
	0	3.43	11.75	20.07	0.29	216	0.1	85 000[a]–70 000[b]
	1	2.73	12.50	22.27	0.22	216	0.1	81 000[a]–59 000[b]
	2	2.01	13.25	24.49	0.15	216	0.2	77 000[a]–48 000[b]
	3	1.27	14.00	26.73	0.09	215	0.4	73 000[a]–37 000[b]
SOA set 2	−1	4.53	9.00	13.47	0.50	194	–	–
	0	4.00	9.25	14.50	0.43	189	–	35 000
	1	3.40	9.50	15.60	0.36	184	–	35 000
	2	2.83	9.75	16.67	0.29	179	–	35 000
SOA set 3	−1	5.25	5.00	4.75	1.05	149	–	–
	0	4.70	5.25	5.80	0.90	144	–	35 000
	1	4.20	5.50	6.80	0.76	140	–	35 000
	2	3.65	5.75	7.85	0.63	135	–	35 000
	3	3.15	6.00	8.85	0.52	131	–	35 000
NTVOCs	6	1.22	7.22	7.14	0.16	113	4.75(OMsv)	–

[a] $OM_{sv}.\Delta H_{vap} = \{85\,000 - 4\,000 \times \log(C^*)\}$ J mol^{-1}. [b] $OM_{sv}.\Delta H_{vap} = \{70\,000 - 11\,000 \times \mathrm{Log}(C^*)\}$ J mol^{-1}.

use different kernel functions, to discretize the distribution of the oxidation products according to their log(C^*) and O : C ratios, when functionalization and fragmentation occur. Instead, to reduce the computational burden of the simulations, the model assumes that the oxidation of a given surrogate yields one other surrogate with lower volatility, higher oxygen number and lower carbon number. These properties should be considered as a weighted average of those relative to the complex mixture of compounds arising from functionalization and fragmentation processes. Accordingly, the 1.5D-VBS approach may represent the functionalization and fragmentation processes, while reducing the parameter space and the computational burden. Gas-phase products in the semi-volatile range in set 2 and set 3, once formed, can further react with a rate constant of 4×10^{-11} cm^3 molec^{-1} s^{-1} as proposed by previous studies (Donahue et al., 2013; Grieshop et al., 2009; Robinson et al., 2007), further lowering the volatility of the products by 1 order of magnitude. This implies that for every additional oxidation step, the organic material receives around 0.5 oxygen atoms (Table 1). According to Donahue et al. (2013), while the rate of increase in oxygen atoms does not decrease with the oxidation generation number, the compounds' fragmentation significantly increases. The fragmentation branching ratio has often been parameterized as a function of the compounds' O : C ratios (e.g. fragmentation ratio $= f(\mathrm{O:C}^{(1/\alpha)})$, where α is a positive integer often between 3 and 6 (Jimenez et al., 2009). This results in a general decrease in the OA compounds' carbon number and hence the number of oxygen added per molecule, but not in the O : C ratio or the carbon oxidation state. Therefore, the oxidation of moderately oxygenated NTVOCs, during the first oxidation step, leads to significant functionalization (addition of at least two oxygen atoms) compared to fragmentation, while the further aging of the resulting oxidation products leads to both functionalization and fragmentation. Representing both processes by only one compound imposes a decrease by only one volatility bin and hence a gain of only half an oxygen atom per oxidation. As the modelled species' average carbon number systematically decreases with aging, this approach effectively takes into consideration the compounds' fragmentation. In parallel, the addition of oxygen reflects the compounds' functionalization with aging and the increase in the measured O : C ratio. Therefore, unlike previous 2D-VBS schemes where functionalization and fragmentation are disentangled, the approach of decreasing the number of carbon atoms and increasing the number of oxygen atoms adopted here simultaneously describes both processes.

4 Parameterization methodology

The modelling approach involves two steps.

i. First, we modelled the partitioning of POA for the 11 smog chamber experiments (eight experiments at RH = 50 % and three experiments at RH = 90 %) before aging begins. This step enables constraining the amounts of primary semi-volatile organic matter (OM_{sv}) in the different volatility bins (OM_{sv}.Vol.dist) and the enthalpy of vaporization of the different sur-

rogates ($OM_{sv}.\Delta H_{vap}$). Combinations of OM_{sv}.Vol.dist and $OM_{sv}.\Delta H_{vap}$ of primary biomass-burning semi-volatile compounds are reported in May et al. (2013), obtained based on thermodenuder data. Several combinations of $OM_{sv}.\Delta H_{vap}$ and OM_{sv}.Vol.dist were tested. The amount of OM_{sv} was varied until the measured POA mass at $t = 0$ ($OA_{t=0}$) was reached and the resulting NTVOCs / OM_{sv} was calculated for the different experiments. The average NTVOCs / OM_{sv} calculated at high and low temperatures were then compared and only combinations of $OM_{sv}.\Delta H_{vap}$ and OM_{sv}.Vol.dist that yielded similar NTVOCs / OM_{sv} ratios at low and high temperatures were considered to fit our data within our experimental variability.

ii. Second, the obtained volatility distributions were used to model the aging of the emissions and SOA formation within the hybrid 1.5D-VBS framework. The time-dependent OA mass and O : C ratios were used as model constraints and the NTVOC reaction rates ($k_{OH\text{-}NTVOCs}$) and yields (Y) as well as average enthalpy of evaporation for secondary material in set 2 and 3 ($SOA.\Delta H_{vap}$) were retrieved. In section 6 we will discuss how other a priori assumed parameters influence the results. For the second step, only experiments performed at RH = 50 % were used, as high RH might favour further uptake of oxygenated secondary organic material into the bulk phase, effectively increasing aerosol yields (Zuend and Seinfeld, 2012). Such effects are beyond the scope of this study.

5 Results

5.1 Inferred OMsv and NTVOCs/OMsv ratios from measurements and partitioning theory

Based on the PTR-ToF-MS and AMS measurements of gas and particle phase organic material at $t = 0$, we seek to determine the ratio NTVOCs / OM_{sv} and the $OM_{sv}.\Delta H_{vap}$ that represent best the observations at high and low temperatures. Combinations of enthalpies of vaporization and volatility distributions of primary biomass-burning semi-volatile compounds are reported in May et al. (2013), based on thermodenuder data. We note that in the current version of the 1.5D-VBS the volatility distribution (Table 1), subsequently referred to as $OM_{sv}.Vol.dist_{REF}$, is used in combination with $OM_{sv}.\Delta H_{vap} = \{85\,000 - 4000 \times \log(C^*)\}\,J\,mol^{-1}$, based on the recommendations of May et al. (2013). Here, several combinations of $OM_{sv}.\Delta H_{vap}$ functions and OM_{sv}.Vol.dist were tested.

In Table 2, the measured $OA_{t=0}$ for all the 11 experiments, which ranges from 6.0 to 22.6 µg m^{-3}, are reported. The OM_{sv} values that match the measured $OA_{t=0}$ are shown as an example for the cases when $OM_{sv}.\Delta H_{vap} = \{85\,000 - 4000 \times \log(C^*)\}\,J\,mol^{-1}$ and

Table 2. Modelled and experimental data for 11 wood-burning experiments. The OM_{sv} mass at the beginning of each chamber experiment is reported together with the measured $OA_{t=0}$ and the initial NTVOCs concentration. NTVOCs / OM_{sv} is the ratio between the measured NTVOCs and the calculated OM_{sv} mass at the beginning of each experiment for the two different $OM_{sv}.\Delta H_{vap}$ functions: [a] $OM_{sv}.\Delta H_{vap} = \{85\,000 - 4000 \times Log(C^*)\}\,J\,mol^{-1}$ and [b] $OM_{sv}.\Delta H_{vap} = \{70\,000 - 11\,000 \times Log(C^*)\}\,J\,mol^{-1}$, used in combination with $OM_{sv}.Vol.dist_{REF}$ presented in Table 1.

	Exp1 $T = 263$ K RH = 50 %	Exp2 $T = 263$ K RH = 50 %	Exp3 $T = 263$ K RH = 50 %	Exp4 $T = 263$ K RH = 90 %	Exp5 $T = 263$ K RH = 90 %	Exp6 $T = 263$ K RH = 90 %	Exp7 $T = 263$ K RH = 90 %	Exp8 $T = 288$ K RH = 50 %	Exp9 $T = 288$ K RH = 50 %	Exp10 $T = 288$ K RH = 50 %	Exp11 $T = 288$ K RH = 50 %
Measured NTVOCs [µg m^{-3}]	185.1	–	–	79.3	143.5	91.7	68.7	121.5	190.4	174.6	195.7
Measured $OA_{t=0}$ [µg m^{-3}]	12.3	8.1	16.7	9.3	12.0	17.7	6.0	22.6	17.5	18.7	18.6
Modelled OM_{sv}^{a} [µg m^{-3}]	17.3	12.1	22.4	13.6	16.9	23.5	9.5	46.6	37.7	39.8	39.6
Modelled OM_{sv}^{b} [µg m^{-3}]	22.7	15.8	29.5	17.8	22.2	31.0	12.3	49.7	40.1	42.4	42.2
(NTVOCs) / $(OM_{sv})^{a}$	10.7	–	–	5.1	8.5	3.9	7.2	2.6	5.0	4.4	4.9
(NTVOCs) / $(OM_{sv})^{b}$	8.1	–	–	4.4	6.4	3.0	5.6	2.4	4.7	4.1	4.6

Table 3. Solutions used for primary organic aerosol enthalpies of vaporization with averages and standard deviations of the (NTVOCs) / (OM_{sv}) ratio.

ΔH_{vapPOA} ($J\,mol^{-1}$)	(NTVOCs) / (OM_{sv}) Average High-T (288 K)	(NTVOCs) / (OM_{sv}) Average Low-T (263 K)
$\{85\,000 - 4000 \times \log(C^*)\}$	4.2 ± 1.1	7.2 ± 2.6
$\{70\,000 - 11\,000 \times \log(C^*)\}$	4.0 ± 1.1	5.5 ± 2.0

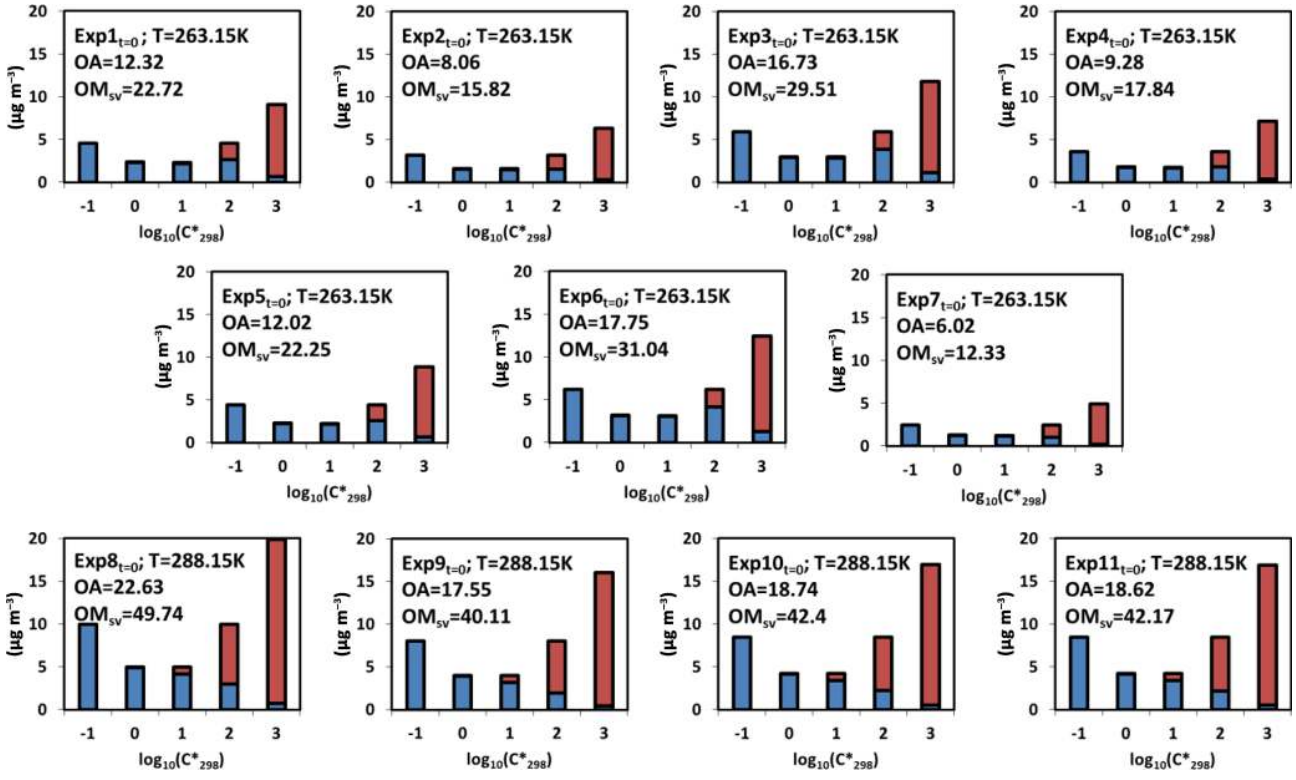

Figure 2. Partitioning of wood-burning POA before the start of the aging for 11 smog chamber experiments (SOL2). Gas phase in red and particle phase in blue.

$OM_{sv}.\Delta H_{vap} = \{70\,000 - 11\,000 \times \log(C^*)\}\,J\,mol^{-1}$ were used in combination with $OM_{sv}.Vol.dist_{REF}$. The average NTVOCs / OM_{sv} ratios obtained using both $OM_{sv}.\Delta H_{vap}$ functions are compared at high and low temperatures in Table 3. $OM_{sv}.\Delta H_{vap} = \{70\,000 - 11\,000 \times \log(C^*)\}\,J\,mol^{-1}$ reduced the observed difference in the average NTVOCs / OM_{sv} ratios at the two temperatures. In general, functions with lowest $OM_{sv}.\Delta H_{vap}$ better explained the change in the measured $OA_{t=0}$ with temperature, with $OM_{sv}.\Delta H_{vap} = \{70\,000 - 11\,000 \times Log(C^*)\}\,J\,mol^{-1}$ best fitting our data. The volatility distributions that could explain our observation have an aggregate contribution in the volatility bins $\log(C^*) = 1$ and 2 smaller than or equal to 0.3. In the following, $OM_{sv}.\Delta H_{vap} = \{70\,000 - 11\,000 \times \log(C^*)\}\,J\,mol^{-1}$ shall be used in combination with $OM_{sv}.Vol.dist_{REF}$ as model inputs and in Sect. 6 we assess the sensitivity of the resulting NTVOCs / OM_{sv} ratios and SOA formed on the chosen $OM_{sv}.Vol.dist$.

Using these model parameters, the overall NTVOCs / OM_{sv} ratio was determined to be around 4.75. Figure 2 shows the resolved equilibrium phase partitioning (Eq. 1) between the gas and particle phase at the beginning of each of the 11 smog chamber experiments ($OA_{t=0}$). As expected, most of the material is found in the gas phase at high temperatures, while at lower temperature only part of the compounds with saturation concentrations (at 20 °C) between 100 and 1000 $\mu g\,m^{-3}$ would reside in the gas phase.

5.2 Wood-burning aging at low and high temperatures

In this section, we will focus on emission aging. Using the NTVOCs / OM_{sv} ratio and the enthalpies of vaporization retrieved in the previous sections, we modelled the eight different smog chamber experiments: nos. 1, 2, 3, and 4 (low temperature) and nos. 8, 9, 10, and 11 (high temperature) performed at the same relative humidity (RH = 50 %). For each of the eight experiments, we injected an average mixture of NTVOCs equal to 4.75 times the OM_{sv} mass before the start of the aging. NTVOCs react solely with OH, whose concentration was retrieved from PTR-MS measurements. The temperature dependence of the reaction rates was also taken into account through the Arrhenius equation. The reaction rates ($k_{OH\text{-}NTVOCs}$) and yields (Y) of the NTVOCs as well as enthalpies of vaporization of SOA ($SOA.\Delta H_{vap}$) in set 2 and set 3 were varied within specific physically realistic ranges that were already proposed in the literature (Koo et al., 2014; Donahue et al., 2013; Grieshop et al., 2009; Robinson et al., 2007). We varied $k_{OH\text{-}NTVOCs}$ between 2 and 4×10^{-11} cm^3 molec^{-1} s^{-1} in steps of 0.1×10^{-11} cm^3 molec^{-1} s^{-1}, and yields between 0.1 and 0.4 ppm ppm^{-1} in steps of 0.01 ppm ppm^{-1}. The yields refer to the sum of the aerosol yields of the four volatility bins. A naphthalene kernel mass distribution with increasing contribution as a function of $\log(C^*)$ is used to distribute the products in the four bins (Murphy and Pandis, 2009). Values for $SOA.\Delta H_{vap}$ are still highly uncertain. In this study, we explored a wide range of values from 15 000 to 115 000 J mol^{-1} in steps of 20 000 J mol^{-1}. The model performance for each combination of $SOA.\Delta H_{vap}$, Y and $k_{OH\text{-}NTVOCs}$ was evaluated by calculating the root mean square error (RMSE) on both the O : C ratio and OA mass (giving the same weight to both quantities) for the eight experiments (giving the same weight to all experiments), and the best-fitting solution is the one that minimized the RMSE. We performed a total number of 31 248 simulations.

Figure 3 shows the total errors for the OA mass (left side) and O : C ratio (right side) for different $SOA.\Delta H_{vap}$, Y and $k_{OH\text{-}NTVOCs}$. The error on the OA mass varies from a minimum of ∼ 25 % up to more than 60 %, whereas the errors on the O : C ratio are lower, ranging from approximately 15 % up to more than 30 %. For the OA mass, distinct regions with lower errors are visible in the central part of each panel with different $SOA.\Delta H_{vap}$, representing the models that best fit the measured OA. While a similar observation can be made for the O : C ratios, models with high $SOA.\Delta H_{vap}$ tend to reproduce the data less faithfully. The diamonds in Fig. 3 indicate the absolute best-fitting solution ($k_{OH\text{-}NTVOCs} = 4.0 \times 10^{-11}$ cm^3 molec^{-1} s^{-1}; $SOA.\Delta H_{vap} =$ 35 000; $Y = 0.32$ ppm ppm^{-1}, in yellow), and the ones retrieved with a likelihood-ratio test allowing for 10 % error form the best fit (red diamonds). Regions with lower errors are localized for $k_{OH\text{-}NTVOCs} \geq 2.5 \times 10^{-11}$ cm^3 molec^{-1} s^{-1} between $SOA.\Delta H_{vap}$ values of 35 000 and 55 000 J mol^{-1}.

Figure 4 shows the modelled and measured OA mass for all eight experiments. The primary organic aerosol fraction is reported as well as the SOA fraction from SVOCs and higher volatility NTVOCs. All the low-temperature experiments (nos. 1, 2, 3, and 4, left side of the panel) were reproduced very well along with the concentration gradients at the end of each experiment even though the model generally tends to slightly over-predict the final OA concentration and to under-predict the production rate. The POA fraction slightly increases at the very beginning of the aging phase, upon the increase in OA mass. As the experiments proceed, POA decreases as a result of its partitioning to the gas phase and subsequent oxidation. Most of the SOA was predicted to be formed from NTVOCs precursors (78–82 %) and only a minor amount from SVOCs (18–22 %). Meanwhile, at high temperatures, SVOCs contribute more significantly to SOA formation compared to low-temperature experiments, although the majority of SOA still arises from NTVOCs. We note that at higher temperatures the OA mass was slightly under-predicted for experiment nos. 9, 10, and 11, but largely over-predicted for experiment no. 8 (see also Fig. S1). We do not have any experimental evidence to discard experiment no. 8 as an outlier, but sensitivity analysis with excluding this experiment yielded slightly lower $SOA.\Delta H_{vap}$ values (∼ 15 000–35 000 J mol^{-1}).

Comparisons between measured and modelled O : C ratios are reported in Fig. 5. Model and observation results match very well, especially upon aging. However, we note on the one hand that significant differences between measured and modelled O : C ratios at the beginning of the experiments can be observed, without any systematic correlation with the chamber conditions (e.g. OA mass or temperature). These differences may be due to the variable nature of primary biomass smoke emissions, which cannot be accounted for in the model. On the other hand, it is noticeable that the model generally under-predicts the measured POA O : C ratios, suggesting that the parameters describing the O : C of primary emissions are suboptimal. These parameters include mainly the carbon and oxygen numbers of species in set 1, and to a lesser extent the OM_{sv}.Vol.dist and the $OM_{sv}.\Delta H_{vap}$, which are all adopted from previously published data. While this observation suggests the presence of compounds with lower carbon number (higher oxygen number) in the primary aerosols (e.g. $C_6H_{10}O_5$ anhydrous sugars, which contribute ∼ 15 % of the POA; Ulevicius et al., 2016), we believe that we do not have suitable data (e.g. analysis at the molecular level) to propose a more accurate representation of the POA compounds. In addition, the average bias in the POA O : C ratios is < 30 %, well within the experimental uncertainties.

6 Discussions and major conclusions

We performed extensive box-model simulations of wood-burning smog chamber experiments conducted at two dif-

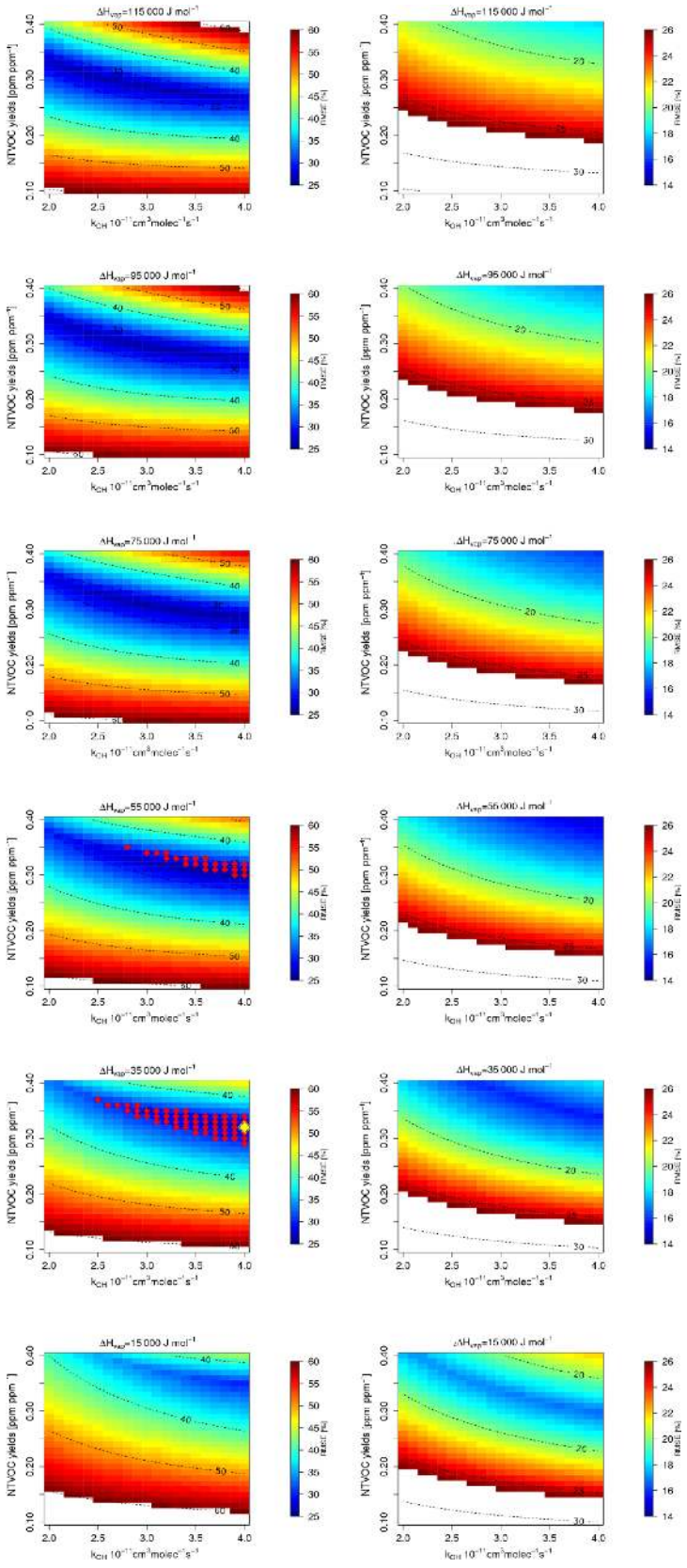

Figure 3. Total error on the OA mass (left side) and on the O : C ratio (right side). White regions have an error larger than 60 % for the OA mass and 26 % for the O : C ratio. The number of simulations per experiment is 3906. The red diamonds indicate the likelihood-ratio test results for solutions within 10 % error from the best one (yellow diamond).

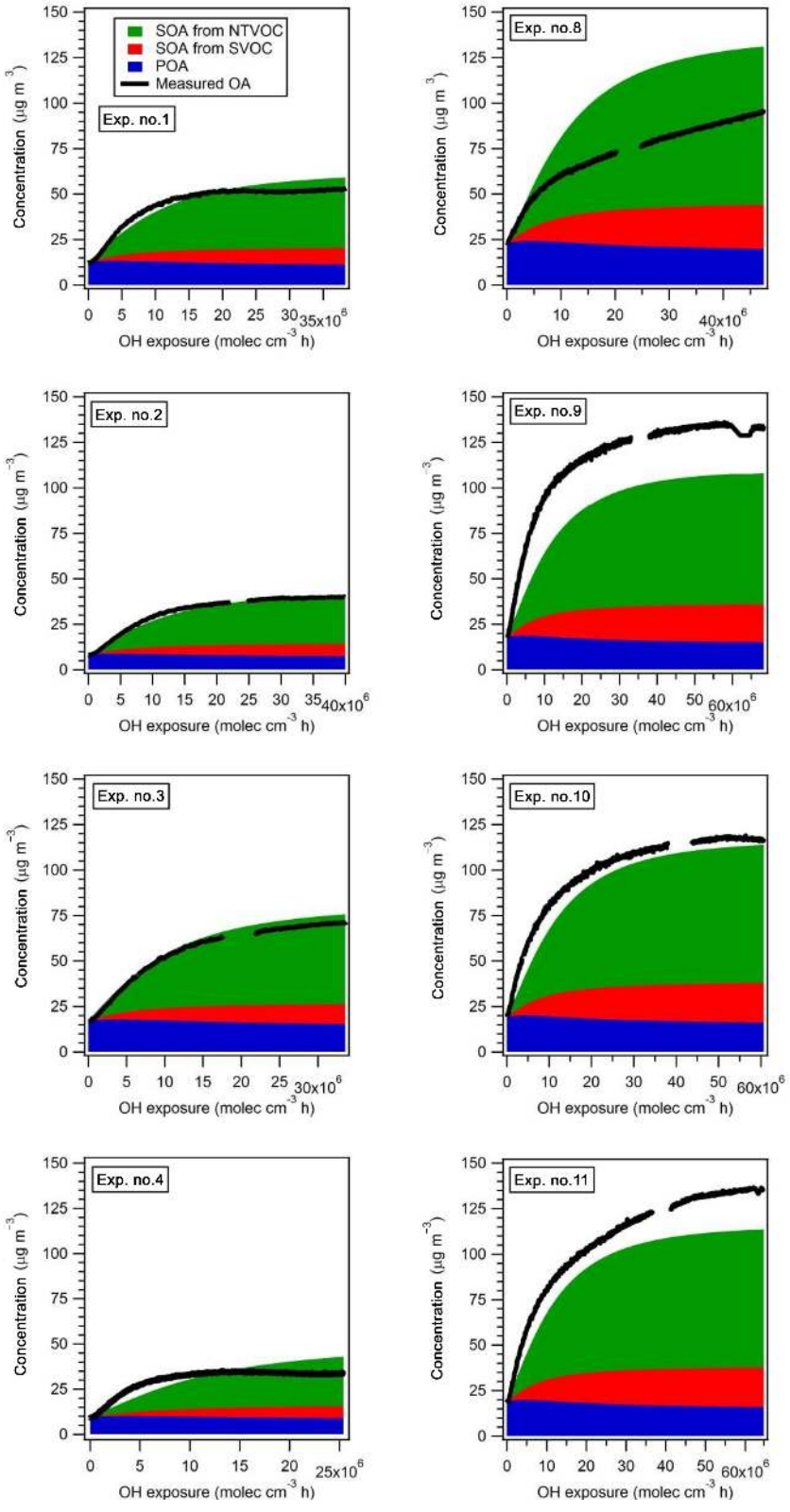

Figure 4. Modelled and observed OA mass for low-temperature experiments (left side) and high-temperature experiments (right side). The model results are for the best-fitting solution (yellow diamond in Fig. 3). SOA from NTVOCs and SVOCs as well as POA are reported in green, red and blue, respectively.

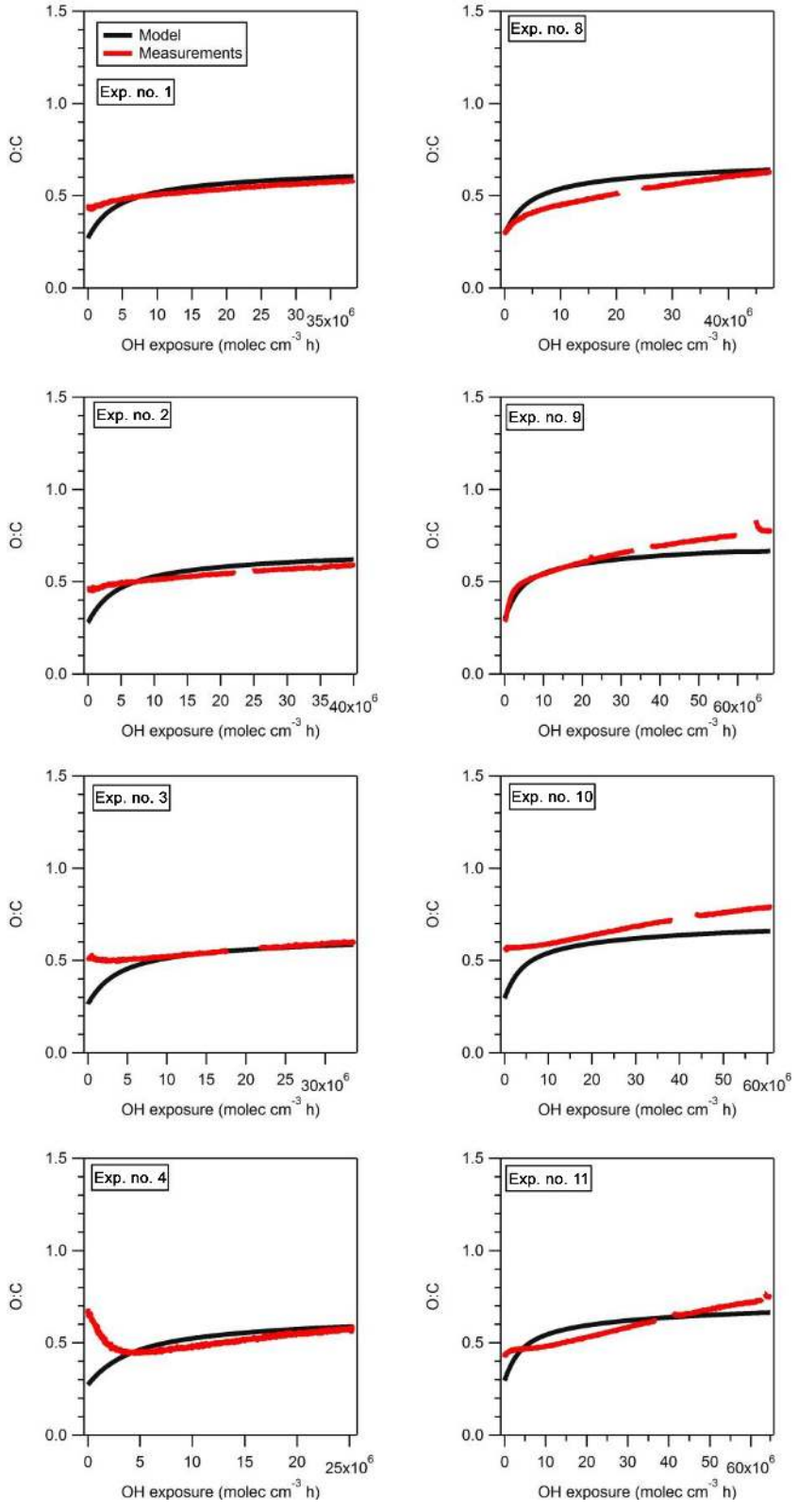

Figure 5. Modelled (black lines) and observed (red lines) O : C ratio for low-temperature experiments (left side) and high-temperature experiments (right side).

ferent temperatures (263 and 288 K). By combining new NTVOCs and organic aerosol measurements we constrained the amounts of NTVOCs that act as SOA precursors. Our estimates indicate that NTVOCs are approximately 4.75 times the amount of total organic material in the 0.1 and 1000 $\mu g\,m^{-3}$ saturation concentration range (OM_{sv}). This ratio can be directly used in CTMs in combination with the proposed aging scheme, in the absence of explicit NTVOCs emissions from wood burning. Our results suggest that only the lowest enthalpies of evaporation of primary SVOCs reported by May et al. (2013) could reproduce the NTVOCs and organic aerosol measurements at both temperatures. These calculations were performed using a single volatility distribution function.

Parameters required for representing SOA formation, such as NTVOCs reaction rates ($k_{OH\text{-}NTVOCs}$), SOA yields (Y) and enthalpies of vaporization of secondary organic aerosol ($SOA.\Delta H_{vap}$), were varied within physically realistic ranges and parameters best fitting the observed OA mass and O : C ratios were retained. The use of time-resolved data and performing the experiments at two different temperatures significantly aided constraining these parameters. Based on the reaction scheme used, best-fitting $k_{OH\text{-}NTVOCs}$ ranged between 3.5 and 4.0×10^{-11} $molec^{-1}\,cm^3\,s^{-1}$, the Y of semi-volatile SOA surrogates ranged between 0.3 and 0.35 $ppm\,ppm^{-1}$, and the $SOA.\Delta H_{vap}$ was determined to be between 35 000 and 55 000 $J\,mol^{-1}$. The model predicted that the majority of the SOA formed during the aging phase arose from NTVOCs and only a small amount from SVOCs.

Many parameters were not varied within the fitting procedure, but a priori assumed. In the following, we discuss the approach used for the selection of these parameters and their influence on the model results. Our results suggest that only the lowest enthalpies of evaporation of primary SVOCs reported by May et al. (2013) could reproduce the NTVOCs and organic aerosol measurements at both temperatures. These low values are consistent with those obtained for SOA ($SOA.\Delta H_{vap} = [35\,000\text{–}55\,000]\,J\,mol^{-1}$ vs. weighted average of $\Delta H_{POA} \sim 50\,000\,J\,mol^{-1}$). Results presented here including the average NTVOCs / OMsv ratios and parameters required for representing SOA formation are all based on the use of one OM_{sv}.Vol.dist. In Fig. S3, we performed a sensitivity analysis where several OM_{sv}.Vol.dist were tested in combination with the same $SOA.\Delta H_{vap}$ function and the same reaction scheme. This analysis shows that the NTVOCs / OM_{sv} ranges between 3.9 and 4.8, which encompasses the value reported here (4.75) and that the resulting SOA is only slightly sensitive to the assumed OM_{sv}.Vol.dist used, especially at low temperature. This is because the OM_{sv} is predicted to contribute to a lesser extent to the measured SOA compared to NTVOCs.

The parameters describing the molecular characteristics (e.g. oxygen and carbon numbers) of the primary SVOCs and their oxidation products (set 1 and 2) were identical to those proposed by Donahue et al. (2012) and Koo et al. (2014). As SVOCs contributed less than NTVOCs to SOA, the modelled OA mass and O : C ratios were not very sensitive to the assumed parameters. Therefore, these assumptions could not be tested and additional measurements at the molecular level would be necessary for better constraining these parameters.

Meanwhile, we have assumed that the volatility distribution of the NTVOCs oxidation products follows the same function as that of naphthalene oxidation products, scaled to fit the total yield Y of these products in the semi-volatility range. Initial tests indicated that the measurements used as constraints did not allow for the determination of the exact shape of this function, due to the limited concentration span during our experiments (within only 1 order of magnitude). Therefore, the function was fixed during the fitting procedure and only the Y was varied. Further experiments spanning a larger range of concentrations would be required for better constraining the volatility distribution of the biomass-burning NTVOCs oxidation products, with a special focus on lower concentrations (between 1 and 20 $\mu g\,m^{-3}$), representative of moderately polluted atmospheres, e.g. in Europe.

The carbon number of the NTVOCs oxidation products was based on the characterization of the chemical nature of these precursors by the PTR-ToF-MS (Bruns et al., 2016), mostly comprising benzene and naphthalene and their methylated derivatives, oxygenated aromatic products and furans with an average carbon number of around 7. Based on Donahue et al. (2013), we have assumed that the oxidation of moderately oxygenated NTVOCs leads to significant functionalization (addition of three oxygens on average), while the further aging of the resulting oxidation products leads to both functionalization and fragmentation. Representing both processes by only one compound in the 1.5D-VBS approach imposed a decrease by only one volatility bin and hence a gain of only one-half oxygen atom per oxidation. This oxidation scheme is different from the one proposed by Donahue et al. (2013), where significant fragmentation occurs with aging combined with the gain of more oxygen atoms. Initial tests showed that a higher increase in the oxygen number with aging would yield a significant decrease of the compounds' volatility ($\sim 1.7 \log(C^*)$ bins per oxygen atom) and hence an overestimation of the increase in SOA yields with aging. An increase of one oxygen atom per oxidation step while decreasing the compounds' volatility by only one bin would imply significant fragmentation with the loss of up to two carbon atoms, impossible in the case of C_6 compounds, especially for low-volatility bins. We have attempted a further increase in the fragmentation compared to the current scheme and the result was an overestimation in the increase of the bulk O : C ratio with aging. We note that the traditional functionalization and fragmentation scheme in the initial VBS was developed by considering SOA precursors to comprise mostly long chain hydrocarbons (e.g. C_{10}–C_{20} alkanes and alkenes), which are expected to be much more subject to fragmentation than aromatics. Therefore, we

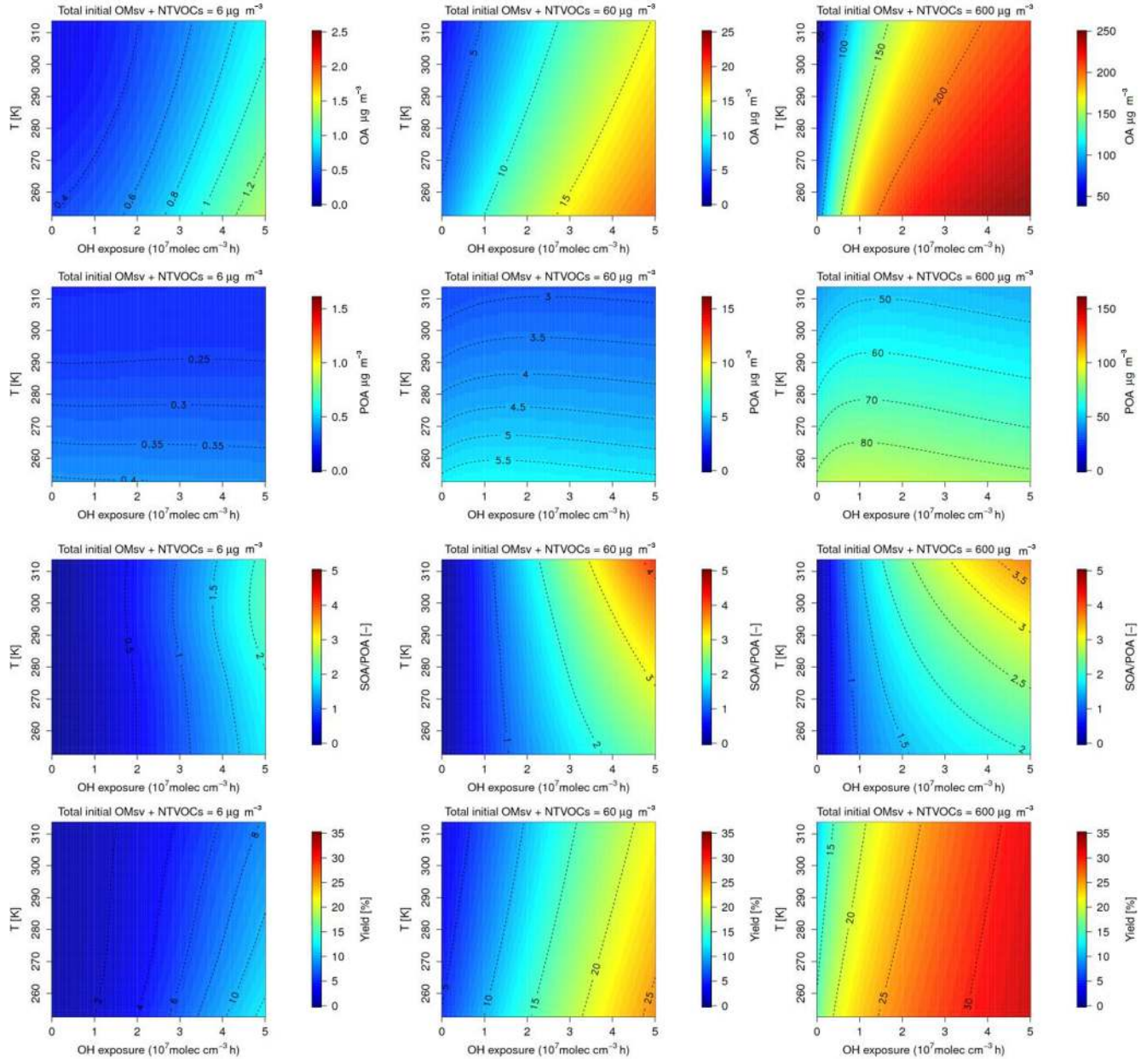

Figure 6. Predicted OA mass (upper panels, note different scales), POA mass, SOA / POA ratio (middle panels) and yields (lower panels) at different OMsv + NTVOCs initial load and atmospheric conditions (T).

consider the scheme proposed here to be more suitable for C_7 aromatic and furan oxidation products.

In the present study, the bulk micro-physical properties of the condensed phase were not measured. Therefore, for all calculations, we assumed instantaneous reversible absorptive equilibrium of semi-volatile organic species into a well-mixed liquid phase; i.e. the model does not invoke diffusion limitations within the condensed phase. These assumptions may influence our results, especially at lower temperatures; e.g. if diffusion limitations were to be considered, higher reaction rates would be required to explain the observations. However, the same assumptions are considered in CTMs and therefore we expect that resulting biases will partially cancel out, providing that the bulk phase properties and condensational sinks of chamber and ambient aerosols are not significantly different.

Based on our best-fitting solutions, the OA mass and composition can be predicted at any given temperature, emission load and OH exposure. This is illustrated in Fig. 6 for three different OM emission loads (OMsv + NTVOCs) of 6, 60 and 600 µg m^{-3} and for a wide range of atmospherically relevant temperatures (from 253.15 to 313.15 K). Partitioning

of POA depends on the temperature and the ambient concentrations.

The POA mass decreases with temperature by 0.5 % K^{-1} on average with higher effects predicted at higher loads (0.7 % K^{-1} at 600 µg m^{-3} vs. 0.3 % at 6 µg m^{-3}). The partitioning coefficient of the primary material increases by about a factor of 1.5 for a 10-fold increase in the emissions. As aging proceeds, POA mass slightly increases as a result of additional partitioning, but after an OH exposure of (1.0–1.5) $\times 10^7$ molec cm^{-3} h, the trend is inverse and POA mass decreases due to the oxidation of semi-volatile primary compounds. This effect is more pronounced at high loads.

From Fig. 6, we can also assess the impact of temperature, OH exposure and emission concentrations on SOA yields. The temperature effect on SOA yields is a function of OH exposure, aerosol load and temperature; i.e. $\partial Y/\partial T = f(T, C_{OA}, OH_{exp})$. SOA yields increase 0.03, 0.06 and 0.05 % K^{-1} on average for 6, 60 and 600 µg m^{-3}, respectively, with higher effects predicted in general at lower temperatures. The temperature effect on the yields is also larger at higher OH exposures (except for very high loads). An analysis typically performed to estimate the volatility distribution of SOA products is based on SOA yields from chamber data performed at different precursor concentrations. We investigated the impact of the OA concentration on the yield at different temperatures and OH exposure. In Fig. S2, an average change in the yield with $\log C_{OA}$ is shown at the different conditions: $(\partial Y/\partial \log C_{OA}) = f(T, OH_{exp})$. An increase in SOA yields with the $\log C_{OA}$ was observed as expected, which is not solely due to additional partitioning, but is also related to changes in the actual chemical composition and hence volatility distribution of the SOA surrogates, as they age to different extents at different concentrations and temperatures. We determined a yield increase of 4–9 percentage points for a 10-fold increase in emissions, with a higher effect at higher OH exposures and lower temperatures.

From Fig. 6, one may also evaluate the minimum OH exposure values required for SOA to exceed POA. SOA is predicted to exceed POA after $\sim 1.5 \times 10^7$ molec cm^{-3} h, for typical ambient concentrations and temperatures. At low temperatures (263 K) and high loads, SOA might exceed POA at an OH exposure of 9×10^6 molec cm^{-3} h, or in 2–10 h (at OH concentrations of (1–5) $\times 10^6$ molec cm^{-3}), in line with previously estimated values for biomass-burning emissions for the typical conditions of haze events (Huang et al., 2014). Comparatively, at 288.15 K an OH exposure of 7×10^6 molec cm^{-3} h would be required for SOA to exceed POA, which might be reached within 2 h or less at typical summer OH concentrations, i.e. (5–10) $\times 10^6$ molec cm^{-3}. These results confirm previous observations during haze events in China that SOA formation is very rapid and SOA mass might exceed primary emissions within timescales of hours, even during haze events (Huang et al., 2014).

Mounting evidence underlines the importance of accurately assessing the emission and evolution of wood-burning emission in the CTMs in order to properly predict the SOA levels retrieved from ambient measurements (Ciarelli et al., 2016; Denier van der Gon et al., 2015; Shrivastava et al., 2015). The simplified VBS scheme proposed here allows for including a mixture of NTVOCs retrieved from latest state-of-the-art wood-burning smog chamber experiments (Bruns et al., 2016). The amount of the new NTVOCs material included in the model was found to be in the range of estimates proposed by previous biomass-burning studies (Shrivastava et al., 2015; Yokelson et al., 2013; Dzepina et al., 2009) and to reproduce most of the chamber experiments successfully. Including the fragmentation and multi-generation chemistry of SOA precursors allows for a reasonable description of the chemical properties of the SOA species including their volatility distribution and their O : C ratios.

The applicability of the parameters to other burning conditions and other emission types should be evaluated in future studies. It has to be noticed that the scheme relies exclusively on chamber experiments conducted with only one type of wood (Beech, *Fagus sylvatica*). Even though the effects of temperature, OH exposure and different emission loads on the predicted OA concentrations were presented in this study, differences in the nature of the emitted organic species (e.g. NTVOCs / OM_{sv} and NTVOC composition) might be expected depending on the different burning conditions and biomass used. Therefore, special care is required when extrapolating the results to a global scale, including more detailed emission information related to the wood-burning habits of the different countries. An application of the proposed scheme, limited to the European scale, can be found in Ciarelli et al. (2017).

Code and data availability. The VBS box model was written in Fortran and was compiled using the Portland group compilers. Simulations were performed under Scientific Linux SL distribution using C shell scripts in order to brute force the chemical and physical parameters. Model output was written in tab-separated text format. Routines to perform the oxidation reactions of SOA precursors and partitioning between particle and gas-phase organic material were taken from the CAMx model (available at http://www.camx.com/) and based on the work of Koo et al. (2014). Please contact the corresponding authors of this publication if you are interested in the model code or applications and/or scientific collaboration.

The Supplement related to this article is available online at https://doi.org/10.5194/gmd-10-2303-2017-supplement.

Competing interests. The authors declare that they have no conflict of interest.

Acknowledgements. This study was financially supported by the Swiss Federal Office of Environment (FOEN). I. El Haddad was financially supported by the Swiss National Science Foundation. We appreciate the availability of the VBS framework in CAMx and support of RAMBOLL ENVIRON.

Edited by: G. Mann
Reviewed by: two anonymous referees

References

Barmet, P., Dommen, J., DeCarlo, P. F., Tritscher, T., Praplan, A. P., Platt, S. M., Prévôt, A. S. H., Donahue, N. M., and Baltensperger, U.: OH clock determination by proton transfer reaction mass spectrometry at an environmental chamber, Atmos. Meas. Tech., 5, 647–656, https://doi.org/10.5194/amt-5-647-2012, 2012.

Bergström, R., Denier van der Gon, H. A. C., Prévôt, A. S. H., Yttri, K. E., and Simpson, D.: Modelling of organic aerosols over Europe (2002–2007) using a volatility basis set (VBS) framework: application of different assumptions regarding the formation of secondary organic aerosol, Atmos. Chem. Phys., 12, 8499–8527, https://doi.org/10.5194/acp-12-8499-2012, 2012.

Bessagnet, B., Colette, A., Meleux, F., Rouïl, L., Ung, A., Favez, O., Thunis, P., Cuvelier, C., Tsyro, S., Stern, R., Manders, A., Kranenburg, R., Aulinger, A., Bieser, J., Mircea, M., Briganti, G., Cappelletti, A., Calori, G., Finardi, S., Silibello, C., Ciarelli, G., Aksoyoglu, S., Prévot, A., Pay, M.-T., Baldasano, J., García Vivanco, M., Garrido, J. L., Palomino, I., Martín, F., Pirovano, G., Roberts, P., Gonzalez, L., White, L., Menut, L., Dupont, J.-C., Carnevale, C., and Pederzoli, A.: The EURODELTA III exercise – Model evaluation with observations issued from the 2009 EMEP intensive period and standard measurements in Feb/Mar 2009, Technical EMEP report 1/2014, Oslo, Norway, 2014.

Bessagnet, B., Pirovano, G., Mircea, M., Cuvelier, C., Aulinger, A., Calori, G., Ciarelli, G., Manders, A., Stern, R., Tsyro, S., García Vivanco, M., Thunis, P., Pay, M.-T., Colette, A., Couvidat, F., Meleux, F., Rouïl, L., Ung, A., Aksoyoglu, S., Baldasano, J. M., Bieser, J., Briganti, G., Cappelletti, A., D'Isidoro, M., Finardi, S., Kranenburg, R., Silibello, C., Carnevale, C., Aas, W., Dupont, J.-C., Fagerli, H., Gonzalez, L., Menut, L., Prévôt, A. S. H., Roberts, P., and White, L.: Presentation of the EURODELTA III intercomparison exercise –evaluation of the chemistry transport models' performance on criteria pollutants and joint analysis with meteorology, Atmos. Chem. Phys., 16, 12667–12701, https://doi.org/10.5194/acp-16-12667-2016, 2016.

Bruns, E. A., Krapf, M., Orasche, J., Huang, Y., Zimmermann, R., Drinovec, L., Mocnik, G., El-Haddad, I., Slowik, J. G., Dommen, J., Baltensperger, U., and Prévôt, A. S. H.: Characterization of primary and secondary wood combustion products generated under different burner loads, Atmos. Chem. Phys., 15, 2825–2841, https://doi.org/10.5194/acp-15-2825-2015, 2015.

Bruns, E. A., El Haddad, I., Slowik, J. G., Kilic, D., Klein, F., Baltensperger, U., and Prévôt, A. S. H.: Identification of significant precursor gases of secondary organic aerosols from residential wood combustion, Sci. Rep., 6, 27881, https://doi.org/10.1038/srep27881, 2016.

Canonaco, F., Slowik, J. G., Baltensperger, U., and Prévôt, A. S. H.: Seasonal differences in oxygenated organic aerosol composition: implications for emissions sources and factor analysis, Atmos. Chem. Phys., 15, 6993–7002, https://doi.org/10.5194/acp-15-6993-2015, 2015.

Ciarelli, G., Aksoyoglu, S., Crippa, M., Jimenez, J.-L., Nemitz, E., Sellegri, K., Äijälä, M., Carbone, S., Mohr, C., O'Dowd, C., Poulain, L., Baltensperger, U., and Prévôt, A. S. H.: Evaluation of European air quality modelled by CAMx including the volatility basis set scheme, Atmos. Chem. Phys., 16, 10313–10332, https://doi.org/10.5194/acp-16-10313-2016, 2016.

Ciarelli, G., Aksoyoglu, S., El Haddad, I., Bruns, E. A., Crippa, M., Poulain, L., Äijälä, M., Carbone, S., Freney, E., O'Dowd, C., Baltensperger, U., and Prévôt, A. S. H.: Modelling winter organic aerosol at the European scale with CAMx: evaluation and source apportionment with a VBS parameterization based on novel wood burning smog chamber experiments, Atmos. Chem. Phys., 17, 7653–7669, https://doi.org/10.5194/acp-17-7653-2017, 2017.

Crippa, M., DeCarlo, P. F., Slowik, J. G., Mohr, C., Heringa, M. F., Chirico, R., Poulain, L., Freutel, F., Sciare, J., Cozic, J., Di Marco, C. F., Elsasser, M., Nicolas, J. B., Marchand, N., Abidi, E., Wiedensohler, A., Drewnick, F., Schneider, J., Borrmann, S., Nemitz, E., Zimmermann, R., Jaffrezo, J.-L., Prévôt, A. S. H., and Baltensperger, U.: Wintertime aerosol chemical composition and source apportionment of the organic fraction in the metropolitan area of Paris, Atmos. Chem. Phys., 13, 961–981, https://doi.org/10.5194/acp-13-961-2013, 2013.

Denier van der Gon, H. A. C., Bergström, R., Fountoukis, C., Johansson, C., Pandis, S. N., Simpson, D., and Visschedijk, A. J. H.: Particulate emissions from residential wood combustion in Europe – revised estimates and an evaluation, Atmos. Chem. Phys., 15, 6503–6519, https://doi.org/10.5194/acp-15-6503-2015, 2015.

Donahue, N. M., Robinson, A. L., Stanier, C. O., and Pandis, S. N.: Coupled Partitioning, Dilution, and Chemical Aging of Semivolatile Organics, Environ. Sci. Technol., 40, 2635–2643, https://doi.org/10.1021/es052297c, 2006.

Donahue, N. M., Epstein, S. A., Pandis, S. N., and Robinson, A. L.: A two-dimensional volatility basis set: 1. organic-aerosol mixing thermodynamics, Atmos. Chem. Phys., 11, 3303–3318, https://doi.org/10.5194/acp-11-3303-2011, 2011.

Donahue, N. M., Kroll, J. H., Pandis, S. N., and Robinson, A. L.: A two-dimensional volatility basis set – Part 2: Diagnostics of organic-aerosol evolution, Atmos. Chem. Phys., 12, 615–634, https://doi.org/10.5194/acp-12-615-2012, 2012.

Donahue, N. M., Chuang, W., Epstein, S. A., Kroll, J. H., Worsnop, D. R., Robinson, A. L., Adams, P. J., and Pandis, S. N.: Why do organic aerosols exist? Understanding aerosol lifetimes using the two-dimensional volatility basis set, Environ. Chem., 10, 151–157, https://doi.org/10.1071/EN13022, 2013.

Drinovec, L., Močnik, G., Zotter, P., Prévôt, A. S. H., Ruckstuhl, C., Coz, E., Rupakheti, M., Sciare, J., Müller, T., Wiedensohler, A., and Hansen, A. D. A.: The "dual-spot" Aethalometer: an improved measurement of aerosol black carbon with real-time loading compensation, Atmos. Meas. Tech., 8, 1965–1979, https://doi.org/10.5194/amt-8-1965-2015, 2015.

Dzepina, K., Volkamer, R. M., Madronich, S., Tulet, P., Ulbrich, I. M., Zhang, Q., Cappa, C. D., Ziemann, P. J., and Jimenez, J. L.: Evaluation of recently-proposed secondary organic aerosol

models for a case study in Mexico City, Atmos. Chem. Phys., 9, 5681–5709, https://doi.org/10.5194/acp-9-5681-2009, 2009.

El Haddad, I., Marchand, N., D'Anna, B., Jaffrezo, J.-L., and Wortham, H.: Functional group composition of organic aerosol from combustion emissions and secondary processes at two contrasted urban environments, Atmos. Environ., 75, 308–320, 2013.

Fountoukis, C., Megaritis, A. G., Skyllakou, K., Charalampidis, P. E., Pilinis, C., Denier van der Gon, H. A. C., Crippa, M., Canonaco, F., Mohr, C., Prévôt, A. S. H., Allan, J. D., Poulain, L., Petäjä, T., Tiitta, P., Carbone, S., Kiendler-Scharr, A., Nemitz, E., O'Dowd, C., Swietlicki, E., and Pandis, S. N.: Organic aerosol concentration and composition over Europe: insights from comparison of regional model predictions with aerosol mass spectrometer factor analysis, Atmos. Chem. Phys., 14, 9061–9076, https://doi.org/10.5194/acp-14-9061-2014, 2014.

Fountoukis, C., Megaritis, A. G., Skyllakou, K., Charalampidis, P. E., Denier van der Gon, H. A. C., Crippa, M., Prévôt, A. S. H., Fachinger, F., Wiedensohler, A., Pilinis, C., and Pandis, S. N.: Simulating the formation of carbonaceous aerosol in a European Megacity (Paris) during the MEGAPOLI summer and winter campaigns, Atmos. Chem. Phys., 16, 3727–3741, https://doi.org/10.5194/acp-16-3727-2016, 2016.

Grieshop, A. P., Logue, J. M., Donahue, N. M., and Robinson, A. L.: Laboratory investigation of photochemical oxidation of organic aerosol from wood fires 1: measurement and simulation of organic aerosol evolution, Atmos. Chem. Phys., 9, 1263–1277, https://doi.org/10.5194/acp-9-1263-2009, 2009.

Heald, C. L., Kroll, J. H., Jimenez, J. L., Docherty, K. S., DeCarlo, P. F., Aiken, A. C., Chen, Q., Martin, S. T., Farmer, D. K., and Artaxo, P.: A simplified description of the evolution of organic aerosol composition in the atmosphere, Geophys. Res. Lett., 37, L08803, https://doi.org/10.1029/2010GL042737, 2010.

Heringa, M. F., DeCarlo, P. F., Chirico, R., Tritscher, T., Clairotte, M., Mohr, C., Crippa, M., Slowik, J. G., Pfaffenberger, L., Dommen, J., Weingartner, E., Prévôt, A. S. H., and Baltensperger, U.: A new method to discriminate secondary organic aerosols from different sources using high-resolution aerosol mass spectra, Atmos. Chem. Phys., 12, 2189–2203, https://doi.org/10.5194/acp-12-2189-2012, 2012.

Hodzic, A., Kasibhatla, P. S., Jo, D. S., Cappa, C. D., Jimenez, J. L., Madronich, S., and Park, R. J.: Rethinking the global secondary organic aerosol (SOA) budget: stronger production, faster removal, shorter lifetime, Atmos. Chem. Phys., 16, 7917–7941, https://doi.org/10.5194/acp-16-7917-2016, 2016.

Huang, R.-J., Zhang, Y., Bozzetti, C., Ho, K.-F., Cao, J.-J., Han, Y., Daellenbach, K. R., Slowik, J. G., Platt, S. M., Canonaco, F., Zotter, P., Wolf, R., Pieber, S. M., Bruns, E. A., Crippa, M., Ciarelli, G., Piazzalunga, A., Schwikowski, M., Abbaszade, G., Schnelle-Kreis, J., Zimmermann, R., An, Z., Szidat, S., Baltensperger, U., Haddad, I. E., and Prévôt, A. S. H.: High secondary aerosol contribution to particulate pollution during haze events in China, Nature, 514, 218–222, https://doi.org/10.1038/nature13774, 2014.

Iinuma, Y., Böge, O., Gräfe, R., and Herrmann, H.: Methyl-Nitrocatechols: Atmospheric Tracer Compounds for Biomass Burning Secondary Organic Aerosols, Environ. Sci. Technol., 44, 8453–8459, https://doi.org/10.1021/es102938a, 2010.

Jathar, S. H., Farina, S. C., Robinson, A. L., and Adams, P. J.: The influence of semi-volatile and reactive primary emissions on the abundance and properties of global organic aerosol, Atmos. Chem. Phys., 11, 7727–7746, https://doi.org/10.5194/acp-11-7727-2011, 2011.

Jimenez, J. L., Canagaratna, M. R., Donahue, N. M., Prevot, A. S. H., Zhang, Q., Kroll, J. H., DeCarlo, P. F., Allan, J. D., Coe, H., Ng, N. L., Aiken, A. C., Docherty, K. S., Ulbrich, I. M., Grieshop, A. P., Robinson, A. L., Duplissy, J., Smith, J. D., Wilson, K. R., Lanz, V. A., Hueglin, C., Sun, Y. L., Tian, J., Laaksonen, A., Raatikainen, T., Rautiainen, J., Vaattovaara, P., Ehn, M., Kulmala, M., Tomlinson, J. M., Collins, D. R., Cubison, M. J., Dunlea, E. J., Huffman, J. A., Onasch, T. B., Alfarra, M. R., Williams, P. I., Bower, K., Kondo, Y., Schneider, J., Drewnick, F., Borrmann, S., Weimer, S., Demerjian, K., Salcedo, D., Cottrell, L., Griffin, R., Takami, A., Miyoshi, T., Hatakeyama, S., Shimono, A., Sun, J. Y., Zhang, Y. M., Dzepina, K., Kimmel, J. R., Sueper, D., Jayne, J. T., Herndon, S. C., Trimborn, A. M., Williams, L. R., Wood, E. C., Middlebrook, A. M., Kolb, C. E., Baltensperger, U., and Worsnop, D. R.: Evolution of organic aerosols in the atmosphere, Science, 326, 1525–1529, https://doi.org/10.1126/science.1180353, 2009.

Kleindienst, T. E., Lewandowski, M., Offenberg, J. H., Jaoui, M., and Edney, E. O.: Ozone-isoprene reaction: Re-examination of the formation of secondary organic aerosol, Geophys. Res. Lett., 34, L01805, https://doi.org/10.1029/2006GL027485, 2007.

Knote, C., Brunner, D., Vogel, H., Allan, J., Asmi, A., Äijälä, M., Carbone, S., van der Gon, H. D., Jimenez, J. L., Kiendler-Scharr, A., Mohr, C., Poulain, L., Prévôt, A. S. H., Swietlicki, E., and Vogel, B.: Towards an online-coupled chemistry-climate model: evaluation of trace gases and aerosols in COSMO-ART, Geosci. Model Dev., 4, 1077–1102, https://doi.org/10.5194/gmd-4-1077-2011, 2011.

Koo, B., Knipping, E., and Yarwood, G.: 1.5-Dimensional volatility basis set approach for modeling organic aerosol in CAMx and CMAQ, Atmos. Environ., 95, 158–164, https://doi.org/10.1016/j.atmosenv.2014.06.031, 2014.

Kostenidou, E., Kaltsonoudis, C., Tsiflikiotou, M., Louvaris, E., Russell, L. M., and Pandis, S. N.: Burning of olive tree branches: a major organic aerosol source in the Mediterranean, Atmos. Chem. Phys., 13, 8797–8811, https://doi.org/10.5194/acp-13-8797-2013, 2013.

Kulmala, M., Asmi, A., Lappalainen, H. K., Carslaw, K. S., Pöschl, U., Baltensperger, U., Hov, Ø., Brenquier, J.-L., Pandis, S. N., Facchini, M. C., Hansson, H.-C., Wiedensohler, A., and O'Dowd, C. D.: Introduction: European Integrated Project on Aerosol Cloud Climate and Air Quality interactions (EUCAARI) – integrating aerosol research from nano to global scales, Atmos. Chem. Phys., 9, 2825–2841, https://doi.org/10.5194/acp-9-2825-2009, 2009.

Kulmala, M., Asmi, A., Lappalainen, H. K., Baltensperger, U., Brenguier, J.-L., Facchini, M. C., Hansson, H.-C., Hov, Ø., O'Dowd, C. D., Pöschl, U., Wiedensohler, A., Boers, R., Boucher, O., de Leeuw, G., Denier van der Gon, H. A. C., Feichter, J., Krejci, R., Laj, P., Lihavainen, H., Lohmann, U., McFiggans, G., Mentel, T., Pilinis, C., Riipinen, I., Schulz, M., Stohl, A., Swietlicki, E., Vignati, E., Alves, C., Amann, M., Ammann, M., Arabas, S., Artaxo, P., Baars, H., Beddows, D. C. S., Bergström, R., Beukes, J. P., Bilde, M., Burkhart, J. F., Canonaco, F., Clegg, S. L., Coe, H., Crumeyrolle, S., D'Anna, B., Decesari, S., Gilardoni, S., Fischer, M., Fjaeraa, A. M., Foun-

toukis, C., George, C., Gomes, L., Halloran, P., Hamburger, T., Harrison, R. M., Herrmann, H., Hoffmann, T., Hoose, C., Hu, M., Hyvärinen, A., Hõrrak, U., Iinuma, Y., Iversen, T., Josipovic, M., Kanakidou, M., Kiendler-Scharr, A., Kirkevåg, A., Kiss, G., Klimont, Z., Kolmonen, P., Komppula, M., Kristjánsson, J.-E., Laakso, L., Laaksonen, A., Labonnote, L., Lanz, V. A., Lehtinen, K. E. J., Rizzo, L. V., Makkonen, R., Manninen, H. E., McMeeking, G., Merikanto, J., Minikin, A., Mirme, S., Morgan, W. T., Nemitz, E., O'Donnell, D., Panwar, T. S., Pawlowska, H., Petzold, A., Pienaar, J. J., Pio, C., Plass-Duelmer, C., Prévôt, A. S. H., Pryor, S., Reddington, C. L., Roberts, G., Rosenfeld, D., Schwarz, J., Seland, Ø., Sellegri, K., Shen, X. J., Shiraiwa, M., Siebert, H., Sierau, B., Simpson, D., Sun, J. Y., Topping, D., Tunved, P., Vaattovaara, P., Vakkari, V., Veefkind, J. P., Visschedijk, A., Vuollekoski, H., Vuolo, R., Wehner, B., Wildt, J., Woodward, S., Worsnop, D. R., van Zadelhoff, G.-J., Zardini, A. A., Zhang, K., van Zyl, P. G., Kerminen, V.-M., S Carslaw, K., and Pandis, S. N.: General overview: European Integrated project on Aerosol Cloud Climate and Air Quality interactions (EUCAARI) – integrating aerosol research from nano to global scales, Atmos. Chem. Phys., 11, 13061–13143, https://doi.org/10.5194/acp-11-13061-2011, 2011.

Lipsky, E. M. and Robinson, A. L.: Effects of Dilution on Fine Particle Mass and Partitioning of Semivolatile Organics in Diesel Exhaust and Wood Smoke, Environ. Sci. Technol., 40, 155–162, https://doi.org/10.1021/es050319p, 2006.

May, A. A., Levin, E. J. T., Hennigan, C. J., Riipinen, I., Lee, T., Collett, J. L., Jimenez, J. L., Kreidenweis, S. M., and Robinson, A. L.: Gas-particle partitioning of primary organic aerosol emissions: 3. Biomass burning, J. Geophys. Res.-Atmos., 118, 11327–11338, https://doi.org/10.1002/jgrd.50828, 2013.

Mohr, C., DeCarlo, P. F., Heringa, M. F., Chirico, R., Slowik, J. G., Richter, R., Reche, C., Alastuey, A., Querol, X., Seco, R., Peñuelas, J., Jiménez, J. L., Crippa, M., Zimmermann, R., Baltensperger, U., and Prévôt, A. S. H.: Identification and quantification of organic aerosol from cooking and other sources in Barcelona using aerosol mass spectrometer data, Atmos. Chem. Phys., 12, 1649–1665, https://doi.org/10.5194/acp-12-1649-2012, 2012.

Murphy, B. N. and Pandis, S. N.: Simulating the Formation of Semivolatile Primary and Secondary Organic Aerosol in a Regional Chemical Transport Model, Environ. Sci. Technol., 43, 4722–4728, https://doi.org/10.1021/es803168a, 2009.

Murphy, B. N., Donahue, N. M., Fountoukis, C., and Pandis, S. N.: Simulating the oxygen content of ambient organic aerosol with the 2D volatility basis set, Atmos. Chem. Phys., 11, 7859–7873, https://doi.org/10.5194/acp-11-7859-2011, 2011.

Nussbaumer, T., Czasch, C., Klippel, N., Johansson, L., and Tullin, C.: Particulate Emissions from Biomass Combustion in IEA Countries, Survey on Measurements and Emission Factors, International Energy Agency (IEA) Bioenergy Task 32, Zurich, Switzerland, 2008a.

Nussbaumer, T., Klippel, N., and Johansson, L.: Survey on Measurements and Emission Factors on Particulate Matter from Biomass Combustion in IEA Countries, 16th European Biomass Conference and Exhibition, 2–6 June 2008, Valencia, Spain, Oral Presentation OA 9.2, 2008b.

Pankow, J. F.: An absorption model of gas/particle partitioning of organic compounds in the atmosphere, Atmos. Environ., 28, 185–188, https://doi.org/10.1016/1352-2310(94)90093-0, 1994.

Pankow, J. F. and Asher, W. E.: SIMPOL.1: a simple group contribution method for predicting vapor pressures and enthalpies of vaporization of multifunctional organic compounds, Atmos. Chem. Phys., 8, 2773–2796, https://doi.org/10.5194/acp-8-2773-2008, 2008.

Platt, S. M., El Haddad, I., Zardini, A. A., Clairotte, M., Astorga, C., Wolf, R., Slowik, J. G., Temime-Roussel, B., Marchand, N., Ježek, I., Drinovec, L., Mocnik, G., Möhler, O., Richter, R., Barmet, P., Bianchi, F., Baltensperger, U., and Prévôt, A. S. H.: Secondary organic aerosol formation from gasoline vehicle emissions in a new mobile environmental reaction chamber, Atmos. Chem. Phys., 13, 9141–9158, https://doi.org/10.5194/acp-13-9141-2013, 2013.

Robinson, A. L., Donahue, N. M., Shrivastava, M. K., Weitkamp, E. A., Sage, A. M., Grieshop, A. P., Lane, T. E., Pierce, J. R., and Pandis, S. N.: Rethinking Organic Aerosols: Semivolatile Emissions and Photochemical Aging, Science, 315, 1259–1262, https://doi.org/10.1126/science.1133061, 2007.

Shrivastava, M. K., Easter, R., Liu, X., Zelenyuk, A., Singh, B., Zhang, K., Ma, P.-L., Chand, D., Ghan, S., Jimenez, J. L., Zhang, Q., Fast, J., Rasch, P., and Tiitta, P.: Global transformation and fate of SOA: Implications of low volatility SOA and gasphase fragmentation reactions, J. Geophys. Res.-Atmos., 120, 4169–4195, https://doi.org/10.1002/2014JD022563, 2015.

Tørseth, K., Aas, W., Breivik, K., Fjæraa, A. M., Fiebig, M., Hjellbrekke, A. G., Lund Myhre, C., Solberg, S., and Yttri, K. E.: Introduction to the European Monitoring and Evaluation Programme (EMEP) and observed atmospheric composition change during 1972–2009, Atmos. Chem. Phys., 12, 5447–5481, https://doi.org/10.5194/acp-12-5447-2012, 2012.

Tsigaridis, K., Daskalakis, N., Kanakidou, M., Adams, P. J., Artaxo, P., Bahadur, R., Balkanski, Y., Bauer, S. E., Bellouin, N., Benedetti, A., Bergman, T., Berntsen, T. K., Beukes, J. P., Bian, H., Carslaw, K. S., Chin, M., Curci, G., Diehl, T., Easter, R. C., Ghan, S. J., Gong, S. L., Hodzic, A., Hoyle, C. R., Iversen, T., Jathar, S., Jimenez, J. L., Kaiser, J. W., Kirkevåg, A., Koch, D., Kokkola, H., Lee, Y. H., Lin, G., Liu, X., Luo, G., Ma, X., Mann, G. W., Mihalopoulos, N., Morcrette, J.-J., Müller, J.-F., Myhre, G., Myriokefalitakis, S., Ng, N. L., O'Donnell, D., Penner, J. E., Pozzoli, L., Pringle, K. J., Russell, L. M., Schulz, M., Sciare, J., Seland, Ø., Shindell, D. T., Sillman, S., Skeie, R. B., Spracklen, D., Stavrakou, T., Steenrod, S. D., Takemura, T., Tiitta, P., Tilmes, S., Tost, H., van Noije, T., van Zyl, P. G., von Salzen, K., Yu, F., Wang, Z., Wang, Z., Zaveri, R. A., Zhang, H., Zhang, K., Zhang, Q., and Zhang, X.: The AeroCom evaluation and intercomparison of organic aerosol in global models, Atmos. Chem. Phys., 14, 10845–10895, https://doi.org/10.5194/acp-14-10845-2014, 2014.

Tsimpidi, A. P., Karydis, V. A., Zavala, M., Lei, W., Molina, L., Ulbrich, I. M., Jimenez, J. L., and Pandis, S. N.: Evaluation of the volatility basis-set approach for the simulation of organic aerosol formation in the Mexico City metropolitan area, Atmos. Chem. Phys., 10, 525–546, https://doi.org/10.5194/acp-10-525-2010, 2010.

Tsimpidi, A. P., Karydis, V. A., Pozzer, A., Pandis, S. N., and Lelieveld, J.: ORACLE (v1.0): module to simulate the organic

aerosol composition and evolution in the atmosphere, Geosci. Model Dev., 7, 3153–3172, https://doi.org/10.5194/gmd-7-3153-2014, 2014.

Tsimpidi, A. P., Karydis, V. A., Pandis, S. N., and Lelieveld, J.: Global combustion sources of organic aerosols: model comparison with 84 AMS factor-analysis data sets, Atmos. Chem. Phys., 16, 8939–8962, https://doi.org/10.5194/acp-16-8939-2016, 2016.

Ulevicius, V., Byčenkiene, S., Bozzetti, C., Vlachou, A., Plauškaitė, K., Mordas, G., Dudoitis, V., Abbaszade, G., Remeikis, V., Garbaras, A., Masalaite, A., Blees, J., Fröhlich, R., Dällenbach, K. R., Canonaco, F., Slowik, J. G., Dommen, J., Zimmermann, R., Schnelle-Kreis, J., Salazar, G. A., Agrios, K., Szidat, S., El Haddad, I., and Prévôt, A. S. H.: Fossil and non-fossil source contributions to atmospheric carbonaceous aerosols during extreme spring grassland fires in Eastern Europe, Atmos. Chem. Phys., 16, 5513–5529, https://doi.org/10.5194/acp-16-5513-2016, 2016.

Waked, A., Favez, O., Alleman, L. Y., Piot, C., Petit, J.-E., Delaunay, T., Verlinden, E., Golly, B., Besombes, J.-L., Jaffrezo, J.-L., and Leoz-Garziandia, E.: Source apportionment of PM_{10} in a north-western Europe regional urban background site (Lens, France) using positive matrix factorization and including primary biogenic emissions, Atmos. Chem. Phys., 14, 3325–3346, https://doi.org/10.5194/acp-14-3325-2014, 2014.

Yokelson, R. J., Burling, I. R., Gilman, J. B., Warneke, C., Stockwell, C. E., de Gouw, J., Akagi, S. K., Urbanski, S. P., Veres, P., Roberts, J. M., Kuster, W. C., Reardon, J., Griffith, D. W. T., Johnson, T. J., Hosseini, S., Miller, J. W., Cocker III, D. R., Jung, H., and Weise, D. R.: Coupling field and laboratory measurements to estimate the emission factors of identified and unidentified trace gases for prescribed fires, Atmos. Chem. Phys., 13, 89–116, https://doi.org/10.5194/acp-13-89-2013, 2013.

Zhang, Q. J., Beekmann, M., Drewnick, F., Freutel, F., Schneider, J., Crippa, M., Prevot, A. S. H., Baltensperger, U., Poulain, L., Wiedensohler, A., Sciare, J., Gros, V., Borbon, A., Colomb, A., Michoud, V., Doussin, J.-F., Denier van der Gon, H. A. C., Haeffelin, M., Dupont, J.-C., Siour, G., Petetin, H., Bessagnet, B., Pandis, S. N., Hodzic, A., Sanchez, O., Honoré, C., and Perrussel, O.: Formation of organic aerosol in the Paris region during the MEGAPOLI summer campaign: evaluation of the volatility-basis-set approach within the CHIMERE model, Atmos. Chem. Phys., 13, 5767–5790, https://doi.org/10.5194/acp-13-5767-2013, 2013.

Zhang, X., Cappa, C. D., Jathar, S. H., McVay, R. C., Ensberg, J. J., Kleeman, M. J., and Seinfeld, J. H.: Influence of vapor wall loss in laboratory chambers on yields of secondary organic aerosol, P. Natl. Acad. Sci. USA, 111, 5802–5807, https://doi.org/10.1073/pnas.1404727111, 2014.

Zotter, P., Ciobanu, V. G., Zhang, Y. L., El-Haddad, I., Macchia, M., Daellenbach, K. R., Salazar, G. A., Huang, R.-J., Wacker, L., Hueglin, C., Piazzalunga, A., Fermo, P., Schwikowski, M., Baltensperger, U., Szidat, S., and Prévôt, A. S. H.: Radiocarbon analysis of elemental and organic carbon in Switzerland during winter-smog episodes from 2008 to 2012 – Part 1: Source apportionment and spatial variability, Atmos. Chem. Phys., 14, 13551–13570, https://doi.org/10.5194/acp-14-13551-2014, 2014.

Zuend, A. and Seinfeld, J. H.: Modeling the gas-particle partitioning of secondary organic aerosol: the importance of liquid-liquid phase separation, Atmos. Chem. Phys., 12, 3857–3882, https://doi.org/10.5194/acp-12-3857-2012, 2012.